

# Breaking the Cycle: Short Recurrence and Overshoot of an M9-class Kamchatka Earthquake

Yuji Yagi  \*<sup>1</sup>, Yukitoshi Fukahata  <sup>2</sup>, Ryo Okuwaki  <sup>1</sup>, Tomohiro Takagawa  <sup>3</sup>, Shinji Toda  <sup>4</sup>

<sup>1</sup>Institute of Life and Environmental Sciences, University of Tsukuba, Tennodai 1-1-1, Tsukuba, Ibaraki 305-8572, Japan, <sup>2</sup>Disaster Prevention Research Institute, Kyoto University, Gokasho, Uji, Kyoto, 611-0011, Japan, <sup>3</sup>Tsunami and Storm Surge Research Group, Port and Airport Research Institute, National Institute of Maritime, Port and Aviation Technology, 1-1-3, Nagase, Yokosuka, 239-0826, Japan, <sup>4</sup>International Research Institute of Disaster Science (IRIDeS), Tohoku University, 468-1 Aoba, Aramaki, Aoba-ku, Sendai, 980-8572, Japan

**Author contributions:** *Conceptualization:* YY., Y.F., S.T. *Methodology:* YY., Y.F., R.O., T.T. *Validation:* YY. *Formal Analysis:* YY. *Investigation:* YY., Y.F., R.O., T.T., S.T. *Resources:* YY., Y.F., R.O., T.T., S.T. *Writing - Original draft:* YY., Y.F. *Writing - Review & Editing:* YY., Y.F., R.O., T.T., S.T. *Visualization:* YY., R.O., T.T. *Supervision:* YY. *Project administration:* YY. *Funding acquisition:* YY.

**Abstract** M9-class megathrust earthquakes in subduction zones are generally thought to release slip deficits on the plate interface accumulated over centuries. However, the 2025 Kamchatka earthquake (Mw 8.8–8.9) ruptured nearly the same area as the 1952 Mw 9.0 event, as shown by the aftershock distribution. This unusually short recurrence interval challenges conventional seismic-cycle models. Using a cutting-edge source inversion technique, we analyze seismic data to estimate the spatiotemporal slip-rate evolution of the 2025 event. The results show that the 2025 rupture involved fault slips exceeding 9 m across a broad region from southern Kamchatka to the northern Kuril Islands, which is significantly greater than the plate convergence of about 6 m since 1952, matching the large-slip area of the 1952 event. Slip rates in the large-slip area accelerated twice, probably due to dynamic stress perturbations and complex frictional behaviour, and were followed by low-angle normal-faulting aftershocks suggesting dynamic overshoot. The results indicate that the 2025 earthquake released a substantial amount of the slip deficit that had not been released during the 1952 event. Therefore, the residual strains that remain after a great earthquake and are not considered in current hazard forecasting can lead to shorter recurrence. This finding offers important clues to how great earthquakes release slip deficits and may help develop more physically based long-term forecasts.

Production Editor:  
Tiegan Hobbs  
Handling Editor:  
Kiran Kumar Thingbaijam  
Copy & Layout Editor:  
Hannah F. Mark

Received:  
September 15, 2025  
Accepted:  
November 24, 2025  
Published:  
November 29, 2025

## 1 Introduction

Forecasting of great earthquakes remains one of the central missions in earthquake science. Great earthquakes along subduction zones are understood to occur in order to release cumulative strain that builds up when part of the overriding plate becomes locked to the subducting plate after the last event, allowing strain to accumulate over a wide area until it is released as a catastrophic rupture (e.g. Scholz, 1998). This is the essence of the seismic cycle: strain builds up between earthquakes and is released in a great rupture. The seismic-cycle hypothesis underpins many forecasting efforts, including hazard assessments for the Nankai Trough and the Cascadia subduction zone, where large interplate earthquakes have repeatedly occurred (e.g. Goda and De Risi, 2024; Hashimoto, 2022). However, the recurrence periodicity of great earthquakes has often been questioned: rupture processes may be much more complex than the seismic-cycle hypothesis assumes (e.g. Kagan and Jackson, 1999; Salditch et al., 2020).

The Kamchatka Peninsula along the eastern coast of Russia is one of the most active subduction zones in the world (e.g. Ruppert et al., 2007; Bilek and Lay, 2018), where the Pacific plate subducts beneath the Okhotsk

plate with a convergence rate of about 8 cm/yr (DeMets et al., 2010) (Fig. 1). On 4 November 1952, a magnitude 9-class earthquake occurred off the coast of southern Kamchatka, generating a devastating trans-Pacific tsunami (e.g. Kanamori, 1976; Okal, 1992). Several historical earthquakes are also known to have occurred in this region, including the 1737 earthquake, which ruptured over a broad area like the 1952 earthquake (e.g. MacInnes et al., 2010). Studies of tsunami deposits indicate that tsunamis have repeatedly struck this region (e.g. Pinegina et al., 2020). In the same region, another M9-class earthquake occurred on 29 July 2025. The epicentres of the 1952 and 2025 events are only about 40 km apart (Fig. 1a, b). The aftershock areas of the two events overlap well, each extending about 500 km southwestward from the epicentre.

These two events, separated by a 73-year recurrence interval which is anomalously short in a relative sense for M9-class earthquakes observed globally (e.g. McCaffrey, 2008), provide a rare opportunity to investigate the variability of great earthquake recurrence along a single subduction segment. Because the plate convergence over 73 years at the convergence rate of 8 cm/yr in this region is only about 6 m, the slip deficit accumulated since the last event alone appears insufficient to explain the large fault slip of the M9-class 2025 Kamchatka

\*Corresponding author: yagi-y@geol.tsukuba.ac.jp

earthquake, especially as back-slip inversions suggest incomplete coupling of the plate interface in the inter-seismic period (Bürgmann et al., 2005; Rousset et al., 2023).

In this study, we estimate the seismic source process of the 2025 Kamchatka earthquake using potency density tensor inversion of teleseismic P-wave data, which contain the highest-frequency components among teleseismic records. We then compare the resulting slip distribution of this event with that of the 1952 event. Our results suggest the occurrence of dynamic overshoot, indicating that the short recurrence interval can be partly attributed to the near-complete release of accumulated strain both before and after the 1952 earthquake.

## 2 Data and Methods

### 2.1 Potency Density Tensor Inversion

Potency density, which equals seismic moment density divided by the rigidity, is a general expression of slip (more precisely, displacement discontinuity across a fault surface) within an elastic body. In Potency Density Tensor Inversion (PDTI) of teleseismic body waves (Shimizu et al., 2020), the potency-rate density tensor is represented by a superposition of five basis double-couple components, neglecting the isotropic component for simplicity (Kikuchi and Kanamori, 1991):

$$u_j(t) = \sum_{q=1}^5 \int \dot{P}_q(\boldsymbol{\xi}, t) * [G_{gj}(\boldsymbol{\xi}, t) + \delta G_{qj}(\boldsymbol{\xi}, t)] d\boldsymbol{\xi} + e_j \quad (1)$$

where  $u_j$  denotes the vertical velocity at station  $j$ ,  $\dot{P}_q(\boldsymbol{\xi}, t)$  denotes the potency-rate density of the  $q$ -th basis double-couple at location  $\boldsymbol{\xi}$  on the model plane at time  $t$ ,  $*$  denotes temporal convolution,  $G_{gj}$  denotes the Green's function for the velocity at station  $j$  due to the unit  $q$ -th basis potency-rate density,  $\delta G_{qj}$  denotes the Gaussian modeling error (Yagi and Fukahata, 2011a), and  $e_j$  denotes the observation error also assumed to follow a Gaussian distribution. This formulation mitigates the problems associated with uncertainties in the fault plane (e.g. Ragon et al., 2018) and underground structure (e.g. Spudich et al., 2019), which are critical issues in source process analysis. PDTI takes advantage of the sensitivity of teleseismic body waves to changes in the focal mechanism, allowing us to estimate fault geometry and rupture evolution during the earthquake. Interestingly, teleseismic body-wave analysis, with a formulation that appropriately accounts for Green's function uncertainties, produces detailed coseismic slip distributions well correlated with those from diverse datasets, including near-field strong-motion records, crustal deformation data, and tsunami data, and is therefore one of the methods that best capture the average features of coseismic slip distribution across different inversion approaches (e.g., seismic, geodetic, and tsunami analyses) (see Fig. 7 in Wong et al., 2024).

Time-adaptive smoothing (Yamashita et al., 2022) was applied as prior constraints; the time-adaptive smoothing mitigates stronger smoothing for larger potency rates. The optimal values of the hyperparameters controlling the relative weight between the Green's function error and the strength of smoothing were determined based on the Akaike Bayesian Information Criterion (ABIC) (e.g. Akaike, 1980). This approach enables estimation of solutions without overfitting, even for highly parameterized models (e.g. Sato et al., 2022). Hereafter, potency density and potency-rate density are referred to as slip and slip rate, respectively. Because non-negativity constraints are unadopted, PDTI allows both positive and negative deviations of slip during the rupture process. As a result, the slip integrated over a certain time window may temporarily exceed the final slip value (e.g. Fig. 3c).

### 2.2 Data

The seismic waveform processing procedure followed a method previously validated in PDTI studies (e.g. Yamashita et al., 2022). Vertical-component teleseismic P waves at available stations were downloaded from Seismological Facility for the Advancement of Geoscience (SAGE; see Data and code availability section), and 80 stations at epicentral distances of  $30^\circ$ – $95^\circ$  ( $\sim 3,335$ – $10,554$  km) were selected and used for the inversion analysis. P-wave onsets were manually picked, and stations for which the P-wave onsets could not be reliably identified were excluded. To minimize bias from uneven station density, we adopted an empirical subsampling approach, preferentially retaining stations with high signal clarity in densely covered regions such as California. A high-pass filter with a corner frequency of 0.002 Hz was applied to remove long-period noise, after which the data were converted to velocity waveforms. To match the model's temporal node interval, the data were decimated to a sampling interval of 1.1 s for PDTI. The temporal node interval was adjusted so that the total number of model parameters remained within a computationally feasible range. To verify that the observed waveform characteristics were adequately reproduced, 20 Hz velocity seismograms, processed with an anti-aliasing filter, were compared with the corresponding synthetic waveforms (Fig. S2). For each station, the waveform window used in the inversion was adjusted to cover the period from the P-wave arrival until before the arrival of the PP-wave radiated from the main rupture, or until the Green's function retained sufficient amplitude (corresponding to the time at which 95% of the total P-wave Green's function energy was reached).

### 2.3 Model setup

PDTI mitigates modeling errors associated with uncertainties in the Earth structure and fault geometry by explicitly incorporating Green's function uncertainties that follow a Gaussian distribution (Yagi and Fukahata, 2011a). We also assessed the influence of non-Gaussian errors by examining three different structure models of the source region and three different geometry models

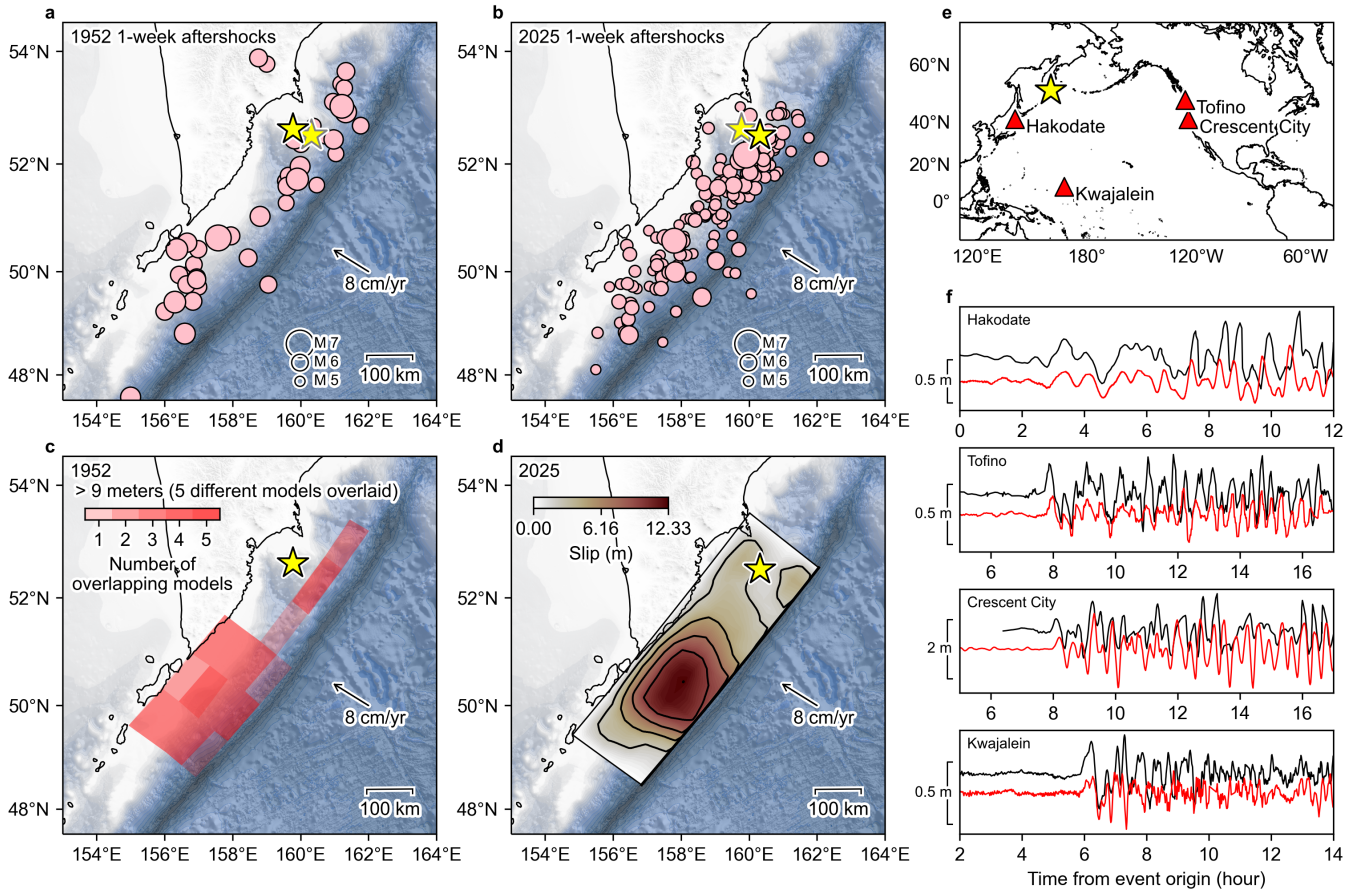


**Figure 1** Comparison of the M9-class 1952 and 2025 Kamchatka earthquakes. (a, b) Aftershocks for the (a) 1952 and (b) 2025 events. The epicentres are from the ANSS ComCat (U.S. Geological Survey Earthquake Hazards Program, 2017) (M 5, 4–11 November 1952; M 5, 29 July–5 August 2025). The black outlined star is the mainshock epicentre of the (a) 1952 and (b) 2025 events. The pink circles are the aftershocks. For comparison, the grey outlined star is the mainshock epicentre of the (a) 2025 and (b) 1952 events. The arrow indicates the plate motion of Pacific plate against Okhotsk plate (DeMets et al., 2010). (c, d) Coseismic slip models for the 1952 and 2025 events. The 1952 model, estimated by MacInnes et al. (2010) utilizing the NOAA’s unit sources with variable dip angles, explains near field tsunami inundation in 1952. Overlapping regions of slip exceeding 9 m are derived from 5 best-fit models that reproduce the inundation, shown in semi-transparent red; darker red indicates a higher degree of model agreement of large slips. The 2025 model is a representative solution of this study, using a dip of 16° and the modified regional structure model of the Kamchatka Peninsula (Table S2). (e) Distribution of the tide-gauge stations. (f) Tsunami waveforms recorded at coastal tide gauges in (e) for the 1952 (black) and 2025 (red) events. A zero-phase high-pass filter with a corner period of three hour was applied to remove tidal effects. Note that the 1952 tsunami waveform at Crescent City is only available from ~6 hours and 24 minutes after the origin time (NOAA National Centers for Environmental Information; NOAA Center for Tsunami Research, 2017). Topography data are from GEBCO\_2025 Grid (GEBCO Compilation Group, 2025).

of the fault plane. Nine analyses were conducted for all combinations of the three velocity models and the three fault geometry models.

The epicentre determined by the U.S. Geological Survey (USGS) (U.S. Geological Survey Earthquake Hazards Program, 2017) was used. The size of the model plane is 550 km × 176 km, with spatial nodes every 25 km and 22 km in the strike and dip directions, respectively. The model fault strike was 218°. Variable cases of the dip angles were examined with the dip-depth combinations of (16°, 30 km), (18°, 33 km), and (20°, 36 km). The initial time node at each spatial node was given by the distance from the hypocentre divided by the virtual rupture front speed of 3.5 km/s, with rupture duration up to 132 s at each spatial node and termination within about 200 s from the initiation of the rupture at every node. One

basis component is taken to coincide with the centroid moment tensor (CMT) in the Global CMT (GCMT) catalog for the 2025 Kamchatka earthquake (strike = 214°, dip = 19°, rake = 87°).

Green’s functions were computed at a sampling interval of 0.1 s using the program of Kikuchi and Kanamori (1991) for three source-region structure models: a modified CRUST1.0 model (Laske et al., 2013) (Table S1), a modified regional structure model of the Kamchatka Peninsula (Nizkous et al., 2007) (Table S2), and a modified AK135 model (Kennett et al., 1995; Montagner and Kennett, 1996) (Table S3). The ray parameter and travel time were computed using TauP (Crotwell et al., 1999) with the AK135 velocity model, and the velocity structure at each station was taken from the AK135 continental crust model.

For comparison with the observed waveforms, synthetic seismograms were computed for all nine models by convolving the 0.1 s-sampled Green's functions for each spatiotemporal node and basis tensor component with the estimated potency-rate density tensor functions, summing the resulting waveforms, and linearly interpolating them to 0.05 s sampling. Focal mechanism information was extracted from the obtained potency-rate density using FPSPACK (Gasperini and Vannucci, 2003).

### 3 Results and Discussion

#### 3.1 Source model of the 2025 Kamchatka earthquake

The moment rate functions exhibit consistent characteristics across all 9 models (Fig. 2c). From the origin time (OT) to OT + 50 s, the initial rupture appears to progress, and the moment rate remains at a low level. The main rupture starts at OT + 50 s. Although it stalls between OT + 65 s and OT + 80 s, the moment rate increases again until OT + 100 s. It then remains at a high level with fluctuation until OT + 160 s, after which it quickly decreases. The resulting seismic moments range from  $1.89 \times 10^{22}$  Nm (Mw 8.8) to  $2.47 \times 10^{22}$  Nm (Mw 8.9). Eight of the nine models show peak slip at depths of approximately 20–40 km (Fig. S1). The synthetic waveforms reproduced by the nine models match the observed velocity waveforms well, including short-period features evident in the 0.05 s-sampled data from stations that were not used in the inversion (Fig. S2).

The main rupture can be divided into four episodes (Fig. 2, S3). Episode 1 (EP1) begins at OT + 50 s in the deeper portion of the fault along strike, 50–175 km southwest from the hypocentre. Episode 2 (EP2) begins at OT + 80 s along strike 150–275 km southwest, propagating to the shallow portion and southward. Episode 3 (EP3) starts at OT + 110 s along strike 230–375 km southwest, extending to all depths. Slip rate peaks are observed around OT + 115 s and OT + 135 s at almost the same along-strike portion, indicating a stagnation in rupture propagation. Episode 4 (EP4) starts at OT + 150 s, propagating along strike 320–460 km southwest.

The cumulative slip distribution reveals that slip exceeding 6 m is observed in an area of 300 km  $\times$  160 km centred around 290 km southwest from the hypocentre in all models, while slip exceeding 9 m is observed, at least partially, within an area of 175 km  $\times$  110 km centred around 325 km southwest in all models (Fig. 3a, b). The maximum slip ranges from 9.6 m to 13.6 m, with a median of 12.1 m (Fig. S4).

One notable feature in the large-slip area is two bursts of slip acceleration during EP3, both at the same location (Fig. 2b, S3). Such characteristics can only be resolved by adopting a source process model with sufficient degrees of freedom to accommodate repeated ruptures. Comparable results are also obtained with a back-projection (BP) method (Fig. S5), which does not impose any a priori constraints on the rupture propagation style. Results from both the PDTI and BP analyses suggest that two episodes of slip acceleration occurred

during EP3 based on the teleseismic P-wave records with the highest temporal resolution. A similar phenomenon was observed during the 2011 Tohoku-Oki earthquake (e.g. Ide et al., 2011; Yagi and Fukahata, 2011b). This reacceleration of slip may be explained either by the limited spatial resolution or by the interaction between dynamic stress perturbations, caused by seismic wave propagation, and complex frictional properties (e.g. Gabuchian et al., 2017; Rubino et al., 2022; Gabriel et al., 2012). While the cumulative slip before the onset of reacceleration was 6–9 m in the large-slip area of EP3, the total slip reached 10–14 m as a result of the reacceleration (Fig. 3c).

The aftershock distribution also shows a conspicuous spatial feature: thrust-type aftershocks are mostly located outside of the large-slip region, while low-angle normal-faulting events, which can be interpreted as polarity-reversed counterparts of thrust-type aftershocks, occurred within the large-slip area (Fig. 3a, b). Before the mainshock, the large-slip area hosted only thrust-type events, where normal-faulting events were not observed (Fig. 4a, b). These low-angle normal-faulting events appear to have been located along the plate interface where the thrust-type events had occurred before the mainshock (Fig. 4c, d). Dynamic overshoot refers to a process in which fault slip exceeds the equilibrium stress level during rupture, resulting in a local reversal of shear stress within the large-slip area (e.g. Oglesby et al., 1998; Oglesby and Day, 2004; Ide et al., 2011). The occurrence of these low-angle normal-faulting aftershocks thus suggests the occurrence of dynamic overshoot of slip in the large-slip area, driven by dynamic stress disturbances, as was also reported for the 2011 Tohoku-Oki earthquake (Ide et al., 2011). It is worth noting that a strike-slip earthquake with a nodal plane nearly parallel to the plate interface also occurred southwest of the low-angle normal-faulting event, in the southwestern part of the large-slip area, suggesting that the shear stress in the plate-convergence direction was nearly zero, consistent with a local stress reversal associated with dynamic overshoot.

#### 3.2 Repeating M9-class earthquake

As shown by the aftershock distribution, the rupture area of the 2025 event is similar to that of the 1952 event (Fig. 1a, b). However, there is a possibility that the two events have complementary slip distributions, meaning that areas unruptured in 1952 had large slip in 2025. In fact, Johnson and Satake (1999), based on tsunami waveform inversion, argued that the 1952 rupture produced large slip concentrated near the southeastern coastline of the Kamchatka Peninsula and the northern Kuril Islands, whereas in this study, the large-slip area of the 2025 event is located farther offshore.

However, in those days, the effects of seawater compressibility, the elasticity of the Earth, and geopotential perturbations, which result in faster simulated tsunami arrival times (e.g. Watada et al., 2014; Baba et al., 2017), were not considered. The lack of consideration of these effects resulted in a northwestward bias of the inferred source location for the 1952 event. In-

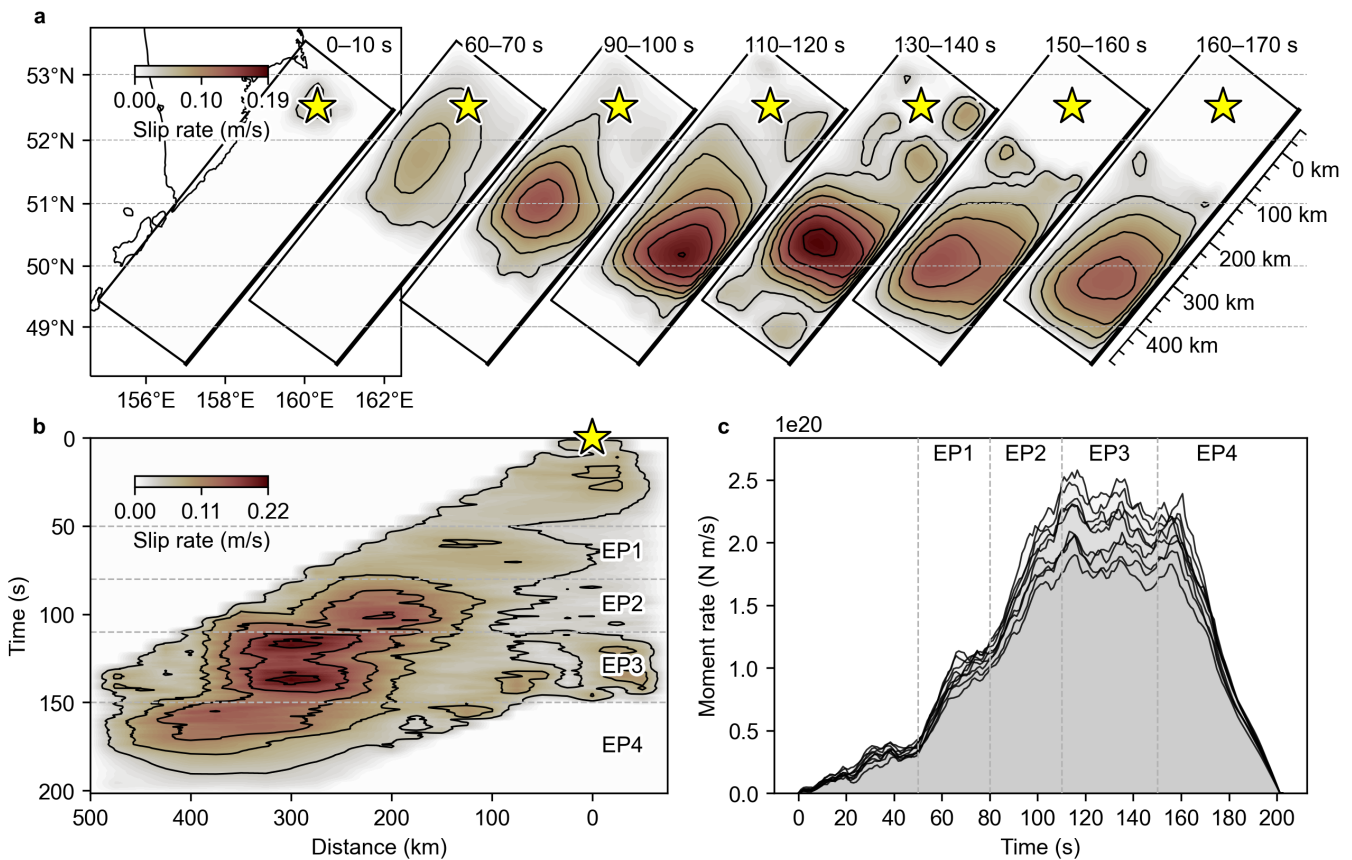


**Figure 2** Rupture growth of the 2025 Kamchatka earthquake. (a, b) Spatiotemporal distribution of slip rate (corresponding to potency-rate density) obtained with a dip of 16° and the modified regional structure model of the Kamchatka Peninsula (Table S2). The star indicates the USGS epicentre of the mainshock. (a) The slip-rate distribution during characteristic time windows is projected onto a map. (b) The temporal evolution of slip rate is projected along the fault-plane strike. Contour intervals are 0.03 m/s for (a) and 0.04 m/s for (b). (c) Moment rate functions obtained for all nine models (Fig. S3).

deed, the tsunami inversion model (Johnson and Satake, 1999) cannot explain near-field tsunami inundation data, which requires large slip in the shallow offshore region from southern Kamchatka to the northern Kuril Islands (MacInnes et al., 2010). This shallow area well corresponds to the region that slipped more than 9 meters during the 2025 event (Fig. 1c, d).

In addition, the 1952 tsunami records digitized from analog data (NOAA National Centers for Environmental Information; NOAA Center for Tsunami Research, 2017) exhibit slightly larger amplitudes than those of the 2025 event, but their overall waveform shapes show a broad similarity during the first 60 minutes (Fig. 1f). When comparing these records, uncertainties in timing need to be kept in mind, and the mismatch becomes more pronounced over time due to changes in bay bathymetry (affecting resonance periods) and differences in tidal conditions. Notably, the amplitudes of the tsunami records in Hawaii differ markedly because the observation sites have changed, while at the Chilean stations the timing is offset by about one hour (Fig. S6). The 2025 tsunami records are well reproduced by models with a tsunami source in the large-slip area identified in this study (NOAA PMEL Center for Tsunami Research, 2025). We conducted tsunami simulations using our estimated source model and confirmed that the major phases of the observed tsunami records are well

reproduced (Text S1, Fig. S7). These findings, together with the similarity of the initial tsunami waveforms between the two events, suggest that the same region is likely to be the main tsunami source for the 1952 event as well.

### 3.3 Dynamic Overshoot and Variability in Earthquake Periodicity

As discussed in the previous section, the slip distributions of the 1952 earthquake and the 2025 earthquake are considered to be similar rather than complementary. This raises the issue of the slip budget, because these two earthquakes occurred only 73 years apart and the slip deficit accumulated on the plate interface is at most about 6 m, based on the plate convergence rate and the interseismic period. On the other hand, as shown in Fig. 3c, the 2025 earthquake has a maximum slip of about 12 m and a displacement of more than 9 m over a wide area.

In general, earthquakes are understood as phenomena that release accumulated tectonic stress. However, rock experiments (e.g. Ohnaka and Yamashita, 1989; Xu et al., 2023), in-situ measurements and their deeper extrapolation (e.g. Townend, 2006) have shown that considerable differential stress remains on the fault surface after a rupture event. In the case of megathrust earth-

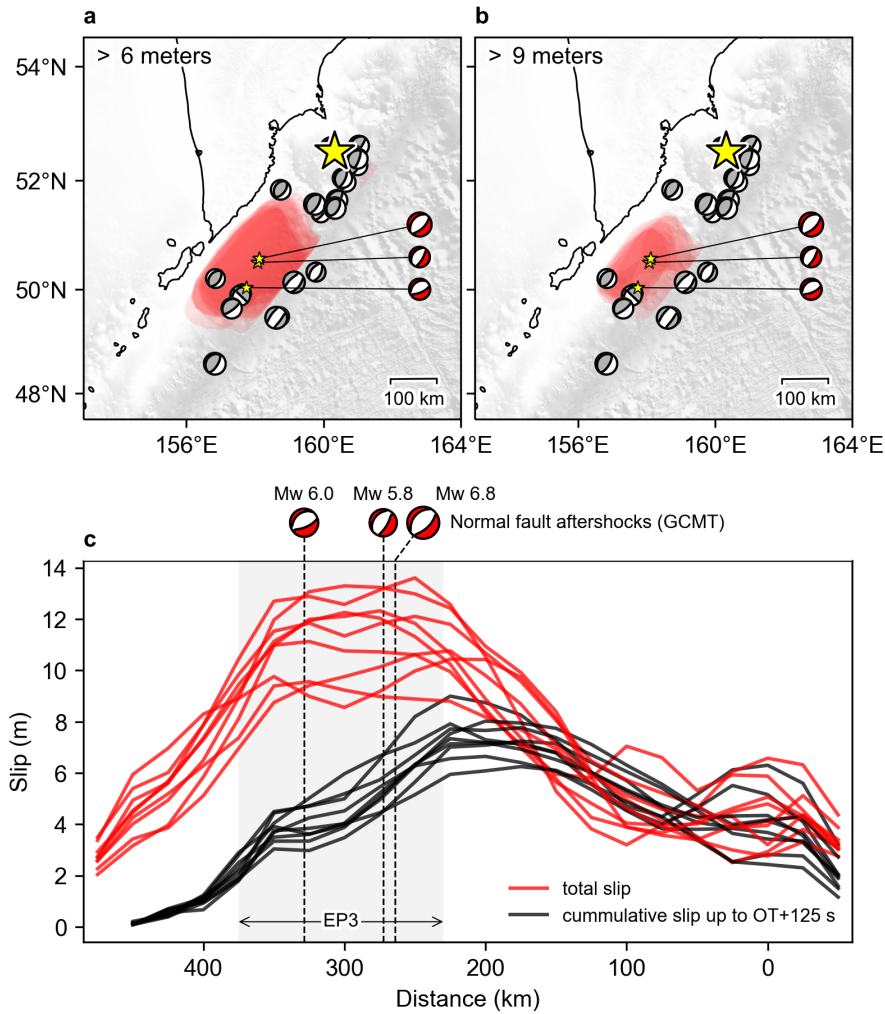


**Figure 3** Coseismic slip distribution for the 2025 event and aftershock moment tensors. (a, b) Overlapping slip areas exceeding 6 m (a) and 9 m (b) for all nine models (Fig. S3). The slip area of each model is shown in semi-transparent red; darker red indicates a higher degree of model agreement of large slips. Beach balls denote moment tensors of the 1-week aftershocks by the Global Centroid Moment Tensor (GCMT) project. Low-angle normal-faulting events are shown in red; others are shown in grey. The star marks the epicentre: the larger one for the 2025 mainshock and the smaller ones for the aftershocks. Topography data from GEBCO\_2025 Grid (GEBCO Compilation Group, 2025). (c) Total slip distribution (red lines) and cumulative slip up to 125 s (black lines), just before the onset of the reacceleration in EP3, both projected along strike. The horizontal axis is the distance from the epicentre along the strike. Each line represents the maximum slip amount at each along-strike grid location.

quakes, they also release the slip deficit accumulated on the plate interface (Reid, 1910), but the slip deficits released by an earthquake would usually be only a portion of the accumulated slip deficits. To account for the above-mentioned gap between the slip amount of the 2025 event and the slip deficit accumulated since the 1952 event, the 2025 event is required to have released not only the post-1952 accumulation but also part of the slip deficit that was not released during the 1952 event. It is deduced that the 1952 event did not completely release the slip deficit accumulated since the 1737 event (e.g. MacInnes et al., 2010), and possibly even earlier ones.

Such an anomalously short recurrence interval for M9-class earthquakes may not be unusual when considered over long timescales. For example, several geological studies, including those using microatolls (e.g. Sieh et al., 2008) and turbidites (e.g. Goldfinger et al., 2013)

for megathrust earthquakes, and paleoseismic trenches across onshore active faults (e.g. Wallace, 1987; Weldon et al., 2004), have shown aperiodicity in inter-event times. These findings suggest that the conventional view of periodic and quasi-periodic occurrences of large earthquakes (e.g. Shimazaki and Nakata, 1980) should be reconsidered. We should recall that even for the well-studied Nankai Trough earthquakes in Japan and the Parkfield earthquakes in the US, for which the time series are well clarified by historical and instrumental records, the periodicity of earthquakes does not hold (e.g. Sykes and Menke, 2006). For example, the intervals of the Nankai Trough earthquakes have changed from 90 to more than 200 years (e.g. Ishibashi, 2004). In the case of the Parkfield earthquakes, while the magnitudes of the earthquakes are nearly constant, the recurrence interval has greatly changed from 12 to 38 years (e.g. Toppozada et al., 2002). In an extreme case, two

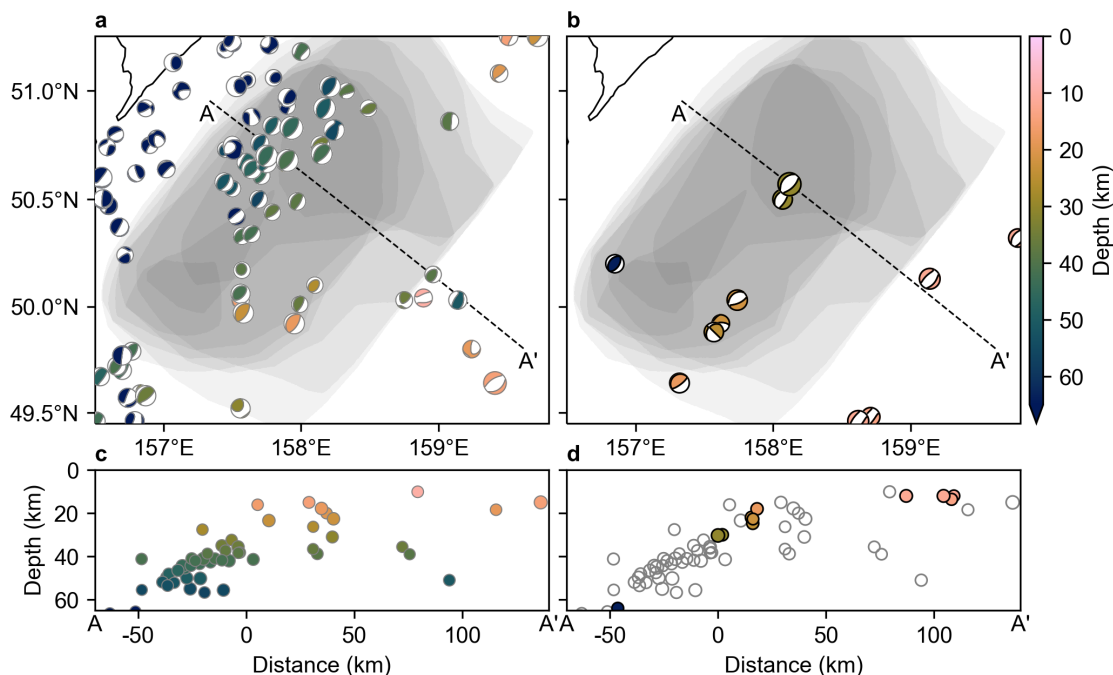


**Figure 4** Moment tensors before and after the 2025 Kamchatka earthquake. (a, b) GCMT moment tensor solutions before (a) and after (b) the 2025 Kamchatka earthquake. The pre-event dataset covers from 1 January 1971 until just before the mainshock; the post-event dataset covers from the mainshock to 5 August 2025. Slip areas exceeding 9 m for all models (Fig. 3b) are shown in semi-transparent grey, with darker colours indicating greater model agreement of more than 9 m slip. (c, d) Cross sections of the GCMT solutions (c) before and (d) after the mainshock. Each solution is projected along the A-A' line on a map. The pre-event GCMT solutions are also plotted in (d) as a circle without colour.

magnitude 6 intraplate earthquakes in northern Kanto, Japan, have occurred on the same active fault only 5.8 years apart (Fukushima et al., 2018). Although such irregularity has often been attributed to interactions with other faults (e.g. Berryman et al., 2012), it seems that significant variation in the amount of slip deficit left behind after each event also plays an important role (e.g. Salditch et al., 2020). In the case of the 2025 Kamchatka earthquake, because no recent large events have occurred in immediately adjacent segments, the effect of fault interaction would be limited, although the 2006 Mw 8.3 Kuril Islands earthquake, whose hypocentre was located more than 300 km southwest of the edge of the 2025 rupture area (U.S. Geological Survey Earthquake Hazards Program, 2017), may have exerted a minor influence.

Our results, particularly the occurrence of low-angle normal-faulting aftershocks within the large-slip area, suggest that dynamic overshoot occurred and that the 2025 Kamchatka earthquake released most of the accumulated stress in the large-slip region. Dynamic stress perturbations and complex frictional properties, including processes such as melting (e.g. Di Toro et al., 2006), flash heating (e.g. Goldsby and Tullis, 2011), and thermal pressurization (e.g. Wibberley and Shimamoto, 2005), may be responsible for such aperiodicity, by changing the remaining stress level after an earthquake. Foreshock activity, such as the magnitude 7.4 event that occurred about 10 days before and 40–50 km northeast of the 2025 Kamchatka epicentre (U.S. Geological Survey Earthquake Hazards Program, 2017), could also af-

fect the timing of gigantic earthquakes, as observed for large continental strike-slip faults triggered by branch faulting (e.g. Stein and Bird, 2024).

If the amount of slip deficit just before and after a megathrust earthquake varies significantly from one earthquake to another, conventional earthquake prediction models that rely solely on accumulated stress, such as the time predictable model and the slip predictable model (Shimazaki and Nakata, 1980), are clearly inapplicable. However, our understanding of the occurrence of earthquakes has continued to advance. For example, Coulomb stress change has proven highly effective in characterizing seismic activity, demonstrating a close link between stress changes and earthquake occurrences (e.g. King et al., 1994; Stein, 1999). Moreover, numerical simulations with detailed structural and fault models have reproduced complex rupture processes (e.g. Taufiqurrahman et al., 2023). Because an earthquake is a process releasing stress accumulated by tectonic motion, quantifying the absolute level of stress and slip deficits on the plate interface would be essential.

## 4 Conclusions

The 2025 Kamchatka earthquake provides an intriguing example: the accumulated slip deficits were almost completely released in the large slip area, where the shear stress dropped to negative values locally, as indicated by the dynamic overshoot. This finding may contribute to clarifying potential mechanisms for fluctua-

tions in the recurrence intervals of megathrust earthquakes, implying that the next M9-class earthquake in this region should occur on a timescale much longer than 73 years. Notably, such complete stress release is uncommon even among M9-class earthquakes; to the best of our knowledge, it has been reported for the 2011 Tohoku-Oki earthquake, but not for the 2004 Sumatra and the 2010 Maule earthquakes. New observational cases, such as the 2025 Kamchatka earthquake, together with their detailed analyses, advance our understanding of megathrust earthquakes and help guide progress toward more physically based long-term forecasting of future destructive earthquakes.

## Acknowledgements

We sincerely thank the editor Kiran Kumar Thingbaijam and the anonymous reviewers for their constructive suggestions and efforts, which greatly improved the quality and clarity of this manuscript. We are grateful to Dr. Breanyn MacInnes for providing the slip data of the 1952 earthquake. Fig. 1c was prepared using the data provided by Dr. Breanyn MacInnes and figures from MacInnes et al. (2010). This research is supported by Japan Society for the promotion of Science (JSPS) Grant-in-Aid for Scientific Research (B) 25K01075.

## Data and code availability

The teleseismic data used in this study were downloaded from SAGE operated by EarthScope via the Wilber 3 system (<https://ds.iris.edu/wilber3/>) including the following station networks: BK (Northern California Earthquake Data Center, 2014), CI (California Institute of Technology and United States Geological Survey Pasadena, 1926), CN (Natural Resources Canada, 1975), CU (Albuquerque Seismological Laboratory (ASL)/USGS, 2006), G (Institut De Physique Du Globe De Paris (IPGP) and Ecole Et Observatoire Des Sciences De La Terre De Strasbourg (EOST), 1982), GE (GEOFON Data Centre, 1993), HK (Hong Kong Observatory, 2009), IC (Albuquerque Seismological Laboratory (ASL)/USGS, 1992), II (Scripps Institution of Oceanography, 1986), IM (Various Institutions, 1965), IU (Albuquerque Seismological Laboratory/USGS, 1988), NL (KNMI, 1993). The USGS events catalog (U.S. Geological Survey Earthquake Hazards Program, 2017) is searched using <https://earthquake.usgs.gov/earthquakes/search/>. The moment tensor solutions of the Global Centroid Moment Tensor (GCMT) catalog (Dziewonski et al., 1981; Ekström et al., 2012) are available through <https://www.globalcmt.org/CMTsearch.html>. The marigrams associated with the 1952 earthquake, excluding those from Hakodate, are available by NOAA Center for Tsunami Research (NOAA PMEL Center for Tsunami Research, 2025). The marigram at Hakodate for the 1952 earthquake is available in Inouye (1953). The sea level data associated with the 2025 earthquake are available by Flanders Marine Institute (VLIZ); Intergovernmental Oceanographic Commission (IOC) (2021). The ak135 and CRUST1.0 are available through websites <https://rses.anu.edu.au/seismology/ak135/ak135f.html>

and <https://igppweb.ucsd.edu/~gabi/crust1.html>, respectively. The source code of Potency Density Tensor Inversion and back projection used in this study is publicly available at [https://github.com/yujiyagi/pdti\\_public\\_version](https://github.com/yujiyagi/pdti_public_version). All figures were generated using Cartopy (Met Office, 2015), Generic Mapping Tools (Wessel et al., 2019), matplotlib (Hunter, 2007), Obspy (Beyreuther et al., 2010), Pyrocko (Heimann et al., 2017), and Scientific colour maps (Crameri, 2023). All scripts and datasets used to generate the figures are publicly available in a Zenodo repository (Yagi et al., 2025). The source codes for the adjoint synthesis method for the tsunami simulation (Takagawa et al., 2024) are archived on Zenodo (Takagawa, 2024) with more recent versions available at <https://github.com/tomographyyy/tandem>. The seafloor displacements for the tsunami simulation are calculated based on the method of Okada (1992) (<https://www.bosai.go.jp/e/dc3d.html>).

## Competing interests

The authors have no competing interests.

## References

- Akaike, H. Likelihood and the Bayes procedure. *Trab. Estad. Y Investig. Oper.*, 31(1):143–166, 1980. doi: 10.1007/BF02888350.
- Albuquerque Seismological Laboratory (ASL)/USGS. New China Digital Seismograph Network, 1992. doi: 10.7914/SN/IC.
- Albuquerque Seismological Laboratory (ASL)/USGS. Caribbean Network, 2006. doi: 10.7914/SN/CU.
- Albuquerque Seismological Laboratory/USGS. Global Seismograph Network (GSN - IRIS/USGS), 1988. doi: 10.7914/SN/IU.
- Baba, T., Allgeyer, S., Hossen, J., Cummins, P. R., Tsushima, H., Imai, K., Yamashita, K., and Kato, T. Accurate numerical simulation of the far-field tsunami caused by the 2011 Tohoku earthquake, including the effects of Boussinesq dispersion, seawater density stratification, elastic loading, and gravitational potential change. *Ocean Model.*, 111:46–54, 2017. doi: 10.1016/j.oceanmod.2017.01.002.
- Berryman, K. R., Cochran, U. A., Clark, K. J., Biasi, G. P., Langridge, R. M., and Villamor, P. Major Earthquakes Occur Regularly on an Isolated Plate Boundary Fault. *Science (80- )*, 336(6089): 1690–1693, jun 2012. doi: 10.1126/science.1218959.
- Beyreuther, M., Barsch, R., Krischer, L., Megies, T., Behr, Y., and Wassermann, J. ObsPy: A Python Toolbox for Seismology. *Seismol. Res. Lett.*, 81(3):530–533, may 2010. doi: 10.1785/gssrl.81.3.530.
- Bilek, S. L. and Lay, T. Subduction zone megathrust earthquakes. *Geosphere*, 14(4):1468–1500, aug 2018. doi: 10.1130/GES01608.1.
- Bürgmann, R., Kogan, M. G., Steblov, G. M., Hilley, G., Levin, V. E., and Apel, E. Interseismic coupling and asperity distribution along the Kamchatka subduction zone. *J. Geophys. Res. Solid Earth*, 110(B7):1–17, jul 2005. doi: 10.1029/2005JB003648.
- California Institute of Technology and United States Geological Survey Pasadena. Southern California Seismic Network, 1926. doi: 10.7914/SN/CI.
- Crameri, F. Scientific colour maps, oct 2023. doi: 10.5281/zenodo.8409685.



- Crotwell, H. P., Owens, T. J., and Ritsema, J. The TauP Toolkit: Flexible Seismic Travel-time and Ray-path Utilities. *Seismol. Res. Lett.*, 70(2):154–160, mar 1999. doi: 10.1785/gssrl.70.2.154.
- DeMets, C., Gordon, R. G., and Argus, D. F. Geologically current plate motions. *Geophysical Journal International*, 181(1):1–80, apr 2010. doi: 10.1111/j.1365-246X.2009.04491.x.
- Di Toro, G., Hirose, T., Nielsen, S., Pennacchioni, G., and Shimamoto, T. Natural and Experimental Evidence of Melt Lubrication of Faults During Earthquakes. *Science (80-. )*, 311(5761):647–649, feb 2006. doi: 10.1126/science.1121012.
- Dziewonski, A. M., Chou, T.-A., and Woodhouse, J. H. Determination of earthquake source parameters from waveform data for studies of global and regional seismicity. *J. Geophys. Res. Solid Earth*, 86(B4):2825–2852, apr 1981. doi: 10.1029/JB086iB04p02825.
- Ekström, G., Nettles, M., and Dziewoński, A. The global CMT project 2004–2010: Centroid-moment tensors for 13,017 earthquakes. *Phys. Earth Planet. Inter.*, 200–201:1–9, jun 2012. doi: 10.1016/j.pepi.2012.04.002.
- Flanders Marine Institute (VLIZ); Intergovernmental Oceanographic Commission (IOC). Sea level station monitoring facility, 2021. doi: 10.14284/482.
- Fukushima, Y., Toda, S., Miura, S., Ishimura, D., Fukuda, J., Demachi, T., and Tachibana, K. Extremely early recurrence of intraplate fault rupture following the Tohoku-Oki earthquake. *Nat. Geosci.*, 11(10):777–781, oct 2018. doi: 10.1038/s41561-018-0201-x.
- Gabriel, A., Ampuero, J., Dalguer, L. A., and Mai, P. M. The transition of dynamic rupture styles in elastic media under velocity-weakening friction. *J. Geophys. Res. Solid Earth*, 117(B9):1–20, sep 2012. doi: 10.1029/2012JB009468.
- Gabuchian, V., Rosakis, A. J., Bhat, H. S., Madariaga, R., and Kanamori, H. Experimental evidence that thrust earthquake ruptures might open faults. *Nature*, 545(7654):336–339, may 2017. doi: 10.1038/nature22045.
- Gasperini, P. and Vannucci, G. FPSPACK: a package of FORTRAN subroutines to manage earthquake focal mechanism data. *Comput. Geosci.*, 29(7):893–901, aug 2003. doi: 10.1016/S0098-3004(03)00096-7.
- GEBCO Compilation Group. GEBCO 2025 Grid, 2025. doi: 10.5285/37c52e96-24ea-67ce-e063-7086abc05f29.
- GEOFON Data Centre. GEOFON Seismic Network, 1993. doi: 10.14470/TR560404.
- Goda, K. and De Risi, R. Time-dependent probabilistic tsunami risk assessment: application to Tofino, British Columbia, Canada, subjected to Cascadia subduction earthquakes. *npj Nat. Hazards*, 1(1):7, may 2024. doi: 10.1038/s44304-024-00006-x.
- Goldfinger, C., Ikeda, Y., Yeats, R. S., and Ren, J. Superquakes and Supercycles. *Seismol. Res. Lett.*, 84(1):24–32, jan 2013. doi: 10.1785/0220110135.
- Goldsby, D. L. and Tullis, T. E. Flash Heating Leads to Low Frictional Strength of Crustal Rocks at Earthquake Slip Rates. *Science (80-. )*, 334(6053):216–218, oct 2011. doi: 10.1126/science.1207902.
- Hashimoto, M. Is the Long-Term Probability of the Occurrence of Large Earthquakes along the Nankai Trough Inflated?—Scientific Review. *Seismol. Res. Lett.*, 93(4):2311–2319, jul 2022. doi: 10.1785/0220210152.
- Heimann, S., Kriegerowski, M., Isken, M., Cesca, S., Daout, S., Grigoli, F., Juretzek, C., Megies, T., Nooshiri, N., Steinberg, A., Sudhaus, H., and Vasyura-Bathke, H. Pyrocko - An open-source seismology toolbox and library, 2017. doi: 10.5880/GFZ.2.1.2017.001.
- Hong Kong Observatory. Hong Kong Seismograph Network, 2009. [http://www.hko.gov.hk/gts/quake/sp\\_seismo\\_network\\_intro\\_e.htm](http://www.hko.gov.hk/gts/quake/sp_seismo_network_intro_e.htm).
- Hunter, J. D. Matplotlib: A 2D Graphics Environment. *Comput. Sci. Eng.*, 9(3):90–95, 2007. doi: 10.1109/MCSE.2007.55.
- Ide, S., Baltay, A., and Beroza, G. C. Shallow Dynamic Overshoot and Energetic Deep Rupture in the 2011 M w 9.0 Tohoku-Oki Earthquake. *Science (80-. )*, 332(6036):1426–1429, jun 2011. doi: 10.1126/science.1207020.
- Inouye, W. Report on the investigation of the Kamchatka earthquake of November 1952 (in Japanese). *Q. J. Seismol.*, 18:5–48, 1953. <https://www.jma.go.jp/jma/kishou/books/kenshin/vol18p005.pdf>.
- Institut De Physique Du Globe De Paris (IPGP) and Ecole Et Observatoire Des Sciences De La Terre De Strasbourg (EOST). GEO-SCOPE, French Global Network of broad band seismic stations, 1982. doi: 10.18715/GEOSCOPE.G.
- Ishibashi, K. Status of historical seismology in Japan. *Ann. Geophys.*, 47(2-3):339–368, dec 2004. doi: 10.4401/ag-3305.
- Johnson, J. M. and Satake, K. Asperity Distribution of the 1952 Great Kamchatka Earthquake and its Relation to Future Earthquake Potential in Kamchatka. *Pure Appl. Geophys.*, 154(3-4):541–553, may 1999. doi: 10.1007/s000240050243.
- Kagan, Y. Y. and Jackson, D. D. Worldwide doublets of large shallow earthquakes. *Bull. Seismol. Soc. Am.*, 89(5):1147–1155, oct 1999. doi: 10.1785/BSSA0890051147.
- Kanamori, H. Re-examination of the earth’s free oscillations excited by the Kamchatka earthquake of November 4, 1952. *Phys. Earth Planet. Inter.*, 11(3):216–226, jan 1976. doi: 10.1016/0031-9201(76)90066-2.
- Kennett, B. L., Engdahl, E. R., and Buland, R. Constraints on seismic velocities in the Earth from traveltimes. *Geophys. J. Int.*, 122(1):108–124, 1995. doi: 10.1111/j.1365-246X.1995.tb03540.x.
- Kikuchi, M. and Kanamori, H. Inversion of complex body waves-III. *Bull. Seism. Soc. Am.*, 81(6):2335–2350, 1991. doi: 10.1785/BSSA0810062335.
- King, G. C. P., Stein, R. S., and Lin, J. Static stress changes and the triggering of earthquakes. *Bull. Seism. Soc. Am.*, 84(3):935–953, 1994. doi: 10.1785/BSSA0840030935.
- KNMI. Netherlands Seismic and Acoustic Network, 1993. doi: 10.21944/E970FD34-23B9-3411-B366-E4F72877D2C5.
- Laske, G., Masters, T. G., Ma, Z., and Pasyanos, M. Update on CRUST1.0 - A 1-degree Global Model of Earth’s Crust. <https://igppweb.ucsd.edu/~gabi/crust1.html>, *Geophys. Res. Abstr.* 15, *Abstr. EGU2013-2658*, 15:Abstract EGU2013–2658, 2013.
- MacInnes, B. T., Weiss, R., Bourgeois, J., and Pinegina, T. K. Slip Distribution of the 1952 Kamchatka Great Earthquake Based on Near-Field Tsunami Deposits and Historical Records. *Bull. Seismol. Soc. Am.*, 100(4):1695–1709, aug 2010. doi: 10.1785/0120090376.
- McCaffrey, R. Global frequency of magnitude 9 earthquakes. *Geology*, 36(3):263–266, mar 2008. doi: 10.1130/G24402A.1.
- Met Office. Cartopy: a cartographic python library with a Matplotlib interface, 2015. doi: 10.5281/zenodo.1182735.
- Montagner, J.-P. and Kennett, B. L. N. How to reconcile body-wave and normal-mode reference earth models. *Geophys. J. Int.*, 125(1):229–248, apr 1996. doi: 10.1111/j.1365-246X.1996.tb06548.x.
- Natural Resources Canada. Canadian National Seismograph Network, 1975. doi: 10.7914/SN/CN.
- Nizkous, I., Kissling, E., Sanina, I., Gontovaya, L., and Levina, V. Correlation of Kamchatka lithosphere velocity anomalies with subduction processes. In *Geophys. Monogr. Ser.*, volume 172, pages

- 97–106. 2007. doi: 10.1029/172GM09.
- NOAA National Centers for Environmental Information; NOAA Center for Tsunami Research. Archival and Discovery of November 4, 1952 Tsunami Event on Marigrams, 2017. doi: 10.7289/V55H7DGQ.
- NOAA PMEL Center for Tsunami Research. Kamchatka Tsunami, July 29, 2025 Main Event Page, 2025. <https://nctr.pmel.noaa.gov/kamchatka20250729/>.
- Northern California Earthquake Data Center. Berkeley Digital Seismic Network (BDSN), 2014. doi: 10.7932/BDSN.
- Oglesby, D. D. and Day, S. M. Fault Geometry and the Dynamics of the 1999 Chi-Chi (Taiwan) Earthquake. *Bull. Seismol. Soc. Am.*, 91(5):1099–1111, oct 2004. doi: 10.1785/0120000714.
- Oglesby, D. D., Archuleta, R. J., and Nielsen, S. B. Earthquakes on Dipping Faults: The Effects of Broken Symmetry. *Science (80-. )*, 280(5366):1055–1059, may 1998. doi: 10.1126/science.280.5366.1055.
- Ohnaka, M. and Yamashita, T. A cohesive zone model for dynamic shear faulting based on experimentally inferred constitutive relation and strong motion source parameters. *J. Geophys. Res. Solid Earth*, 94(B4):4089–4104, apr 1989. doi: 10.1029/JB094iB04p04089.
- Okada, Y. Internal deformation due to shear and tensile faults in a half-space. *Bull. Seismol. Soc. Am.*, 82(2):1018–1040, apr 1992. doi: 10.1785/BSSA0820021018.
- Okal, E. A. Use of the mantle magnitude  $M_m$  for the reassessment of the moment of historical earthquakes. *pure Appl. Geophys.*, 139(1):17–57, mar 1992. doi: 10.1007/BF00876825.
- Pinegina, T., Bourgeois, J., Bazanova, L., Zelenin, E., Krasheninikov, S., and Portnyagin, M. Coseismic coastal subsidence associated with unusually wide rupture of prehistoric earthquakes on the Kamchatka subduction zone: A record in buried erosional scarps and tsunami deposits. *Quat. Sci. Rev.*, 233: 106171, apr 2020. doi: 10.1016/j.quascirev.2020.106171.
- Ragon, T., Sladen, A., and Simons, M. Accounting for uncertain fault geometry in earthquake source inversions - I: Theory and simplified application. *Geophys. J. Int.*, 214(2):1174–1190, 2018. doi: 10.1093/gji/ggy187.
- Reid, H. F. The mechanics of the earthquake, the California earthquake of April 18, 1906. *Rep. State Earthq. Investig. Comm.*, II: 1–192, 1910.
- Rousset, B., Campillo, M., Shapiro, N. M., Walpersdorf, A., Titkov, N., and Chebrov, D. V. The 2013 Slab-Wide Kamchatka Earthquake Sequence. *Geophys. Res. Lett.*, 50(4):1–10, feb 2023. doi: 10.1029/2022GL101856.
- Rubino, V., Lapusta, N., and Rosakis, A. J. Intermittent lab earthquakes in dynamically weakening fault gouge. *Nature*, 606 (7916):922–929, jun 2022. doi: 10.1038/s41586-022-04749-3.
- Ruppert, N. A., Lees, J. M., and Kozyreva, N. P. Seismicity, earthquakes and structure along the Alaska-Aleutian and Kamchatka-Kurile Subduction Zones: A review. In *Volcanism Subduction Kamchatka Reg.*, number February 2015, pages 129–144. 2007. doi: 10.1029/172GM12.
- Salditch, L., Stein, S., Neely, J., Spencer, B. D., Brooks, E. M., Agnon, A., and Liu, M. Earthquake supercycles and Long-Term Fault Memory. *Tectonophysics*, 774(July 2019):228289, jan 2020. doi: 10.1016/j.tecto.2019.228289.
- Sato, D., Fukahata, Y., and Nozue, Y. Appropriate reduction of the posterior distribution in fully Bayesian inversions. *Geophys. J. Int.*, 231(2):950–981, jul 2022. doi: 10.1093/gji/ggac231.
- Scholz, C. H. Earthquakes and friction laws. *Nature*, 391(6662): 37–42, jan 1998. doi: 10.1038/34097.
- Scripps Institution of Oceanography. Global Seismograph Network - IRIS/IDA, 1986. doi: 10.7914/SN/II.
- Shimazaki, K. and Nakata, T. Time-predictable recurrence model for large earthquakes. *Geophys. Res. Lett.*, 7(4):279–282, apr 1980. doi: 10.1029/GL007i004p00279.
- Shimizu, K., Yagi, Y., Okuwaki, R., and Fukahata, Y. Development of an inversion method to extract information on fault geometry from teleseismic data. *Geophysical Journal International*, 220 (2):1055–1065, feb 2020. doi: 10.1093/gji/ggz496.
- Sieh, K., Natawidjaja, D. H., Meltzner, A. J., Shen, C.-C., Cheng, H., Li, K.-S., Suwargadi, B. W., Galetzka, J., Philiposian, B., and Edwards, R. L. Earthquake Supercycles Inferred from Sea-Level Changes Recorded in the Corals of West Sumatra. *Science (80-. )*, 322(5908):1674–1678, dec 2008. doi: 10.1126/science.1163589.
- Spudich, P., Cirella, A., Scognamiglio, L., and Tinti, E. Variability in synthetic earthquake ground motions caused by source variability and errors in wave propagation models. *Geophys. J. Int.*, 219(1):346–372, 2019. doi: 10.1093/gji/ggz275.
- Stein, R. S. The role of stress transfer in earthquake occurrence. *Nature*, 402(6762):605–609, dec 1999. doi: 10.1038/45144.
- Stein, R. S. and Bird, P. Why Do Great Continental Transform Earthquakes Nucleate on Branch Faults? *Seismol. Res. Lett.*, (6): 3406–3415, nov 2024. doi: 10.1785/0220240175.
- Sykes, L. R. and Menke, W. Repeat Times of Large Earthquakes: Implications for Earthquake Mechanics and Long-Term Prediction. *Bull. Seismol. Soc. Am.*, 96(5):1569–1596, oct 2006. doi: 10.1785/0120050083.
- Takagawa, T. tomographyyy/tandem: major release v.1.0.0 [software], Apr. 2024. doi: 10.5281/zenodo.10995292.
- Takagawa, T., Allgeyer, S., and Cummins, P. Adjoint Synthesis for Trans-Oceanic Tsunami Waveforms and Simultaneous Inversion of Fault Geometry and Slip Distribution. *J. Geophys. Res. Solid Earth*, 129(6):e2024JB028750, jun 2024. doi: 10.1029/2024JB028750.
- Taufiqurrahman, T., Gabriel, A.-A., Li, D., Ulrich, T., Li, B., Carena, S., Verdecchia, A., and Gallovič, F. Dynamics, interactions and delays of the 2019 Ridgecrest rupture sequence. *Nature*, 618 (7964):308–315, jun 2023. doi: 10.1038/s41586-023-05985-x.
- Topozada, T. R., Branum, D. M., Reichle, M. S., and Hallstrom, C. L. San Andreas Fault Zone, California:  $M \geq 5.5$  Earthquake History. *Bull. Seismol. Soc. Am.*, 92(7):2555–2601, oct 2002. doi: 10.1785/0120000614.
- Townend, J. What do faults feel? Observational constraints on the stresses acting on seismogenic faults. In *Earthquakes Radiated Energy Phys. Faulting*, pages 313–327. 2006. doi: 10.1029/170GM31.
- U.S. Geological Survey Earthquake Hazards Program. Advanced National Seismic System (ANSS) Comprehensive Catalog of Earthquake Events and Products, 2017. doi: 10.5066/F7MS3QZH.
- Various Institutions. International Miscellaneous Stations, 1965. doi: 10.7914/VEFQ-VH75.
- Wallace, R. E. Grouping and migration of surface faulting and variations in slip rates on faults in the Great Basin province. *Bull. Seismol. Soc. Am.*, 77(3):868–876, jun 1987. doi: 10.1785/BSSA0770030868.
- Watada, S., Kusumoto, S., and Satake, K. Traveltime delay and initial phase reversal of distant tsunamis coupled with the self-gravitating elastic Earth. *J. Geophys. Res. Solid Earth*, 119(5): 4287–4310, may 2014. doi: 10.1002/2013JB010841.
- Weldon, R., Scharer, K., Fumal, T., and Biasi, G. Wrightwood and the earthquake cycle: What a long recurrence record tells us about how faults work. *GSA Today*, 14(9):4, 2004. doi:

10.1130/1052-5173(2004)014<4:WATECW>2.0.CO;2.

Wessel, P., Luis, J. F., Uieda, L., Scharroo, R., Wobbe, F., Smith, W. H. F., and Tian, D. The Generic Mapping Tools Version 6. *Geochemistry, Geophys. Geosystems*, 20(11):5556–5564, nov 2019. doi: 10.1029/2019GC008515.

Wibberley, C. A. J. and Shimamoto, T. Earthquake slip weakening and asperities explained by thermal pressurization. *Nature*, 436(7051):689–692, aug 2005. doi: 10.1038/nature03901.

Wong, J. W. C., Fan, W., and Gabriel, A. A. A Quantitative Comparison and Validation of Finite-Fault Models: The 2011 Tohoku-Oki Earthquake. *J. Geophys. Res. Solid Earth*, 129(10), 2024. doi: 10.1029/2024JB029212.

Xu, S., Fukuyama, E., Yamashita, F., Kawakata, H., Mizoguchi, K., and Takizawa, S. Fault strength and rupture process controlled by fault surface topography. *Nat. Geosci.*, 16(1):94–100, jan 2023. doi: 10.1038/s41561-022-01093-z.

Yagi, Y. and Fukahata, Y. Introduction of uncertainty of Green’s function into waveform inversion for seismic source processes. *Geophysical Journal International*, 186(2):711–720, aug 2011a. doi: 10.1111/j.1365-246X.2011.05043.x.

Yagi, Y. and Fukahata, Y. Rupture process of the 2011 Tohoku-oki earthquake and absolute elastic strain release. *Geophys. Res. Lett.*, 38(19):L19307, oct 2011b. doi: 10.1029/2011GL048701.

Yagi, Y., Fukahata, Y., Okuwaki, R., Takagawa, T., and Toda, S. Archive of processed data and scripts for the source process analyses of the 2025 Kamchatka earthquake [dataset], Oct. 2025. doi: 10.5281/zenodo.17379117.

Yamashita, S., Yagi, Y., Okuwaki, R., Shimizu, K., Agata, R., and Fukahata, Y. Potency density tensor inversion of complex body waveforms with time-adaptive smoothing constraint. *Geophysical Journal International*, 231(1):91–107, jun 2022. doi: 10.1093/gji/ggac181.

The article *Breaking the Cycle: Short Recurrence and Overshoot of an M9-class Kamchatka Earthquake* © 2025 by Yuji Yagi is licensed under CC BY 4.0.